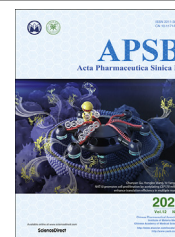




Chinese Pharmaceutical Association
Institute of Materia Medica, Chinese Academy of Medical Sciences

Acta Pharmaceutica Sinica B

www.elsevier.com/locate/apsb
www.sciencedirect.com



ORIGINAL ARTICLE

Hyperthermia based individual *in situ* recombinant vaccine enhances lymph nodes drainage for *de novo* antitumor immunity



Cuixia Zheng^{b,†}, Xinxin Liu^{a,b,†}, Yueyue Kong^b, Lei Zhang^d,
Qingling Song^b, Hongjuan Zhao^b, Lu Han^b, Jiannan Jiao^b,
Qianhua Feng^{b,c,*}, Lei Wang^{a,b,c,e,*}

^aLuoyang Central Hospital Affiliated to Zhengzhou University, Luoyang 471009, China

^bSchool of Pharmaceutical Sciences, Zhengzhou University, Zhengzhou 450001, China

^cKey Laboratory of Advanced Drug Preparation Technologies, Ministry of Education, School of Pharmaceutical Sciences, Zhengzhou University, Zhengzhou 450001, China

^dDepartment of Gynecology, the First Affiliated Hospital of Zhengzhou University, Zhengzhou 450000, China

^eTumor Immunity and Biomaterials Advanced Medical Center, Zhengzhou University, Luoyang 471009, China

Received 7 November 2021; received in revised form 10 January 2022; accepted 12 February 2022

KEY WORDS

Au nanocages;
Simvastatin;
Photothermal therapy;
Tumor-derived protein
antigens;
Recombinant vaccine;
Tumor targeting;
Lymph node drainage;
De novo antitumor
immunity

Abstract The continuing challenges that limit effectiveness of tumor therapeutic vaccines were high heterogeneity of tumor immunogenicity, low bioactivity of antigens, as well as insufficient lymph nodes (LNs) drainage of antigens and adjuvants. Transportation of *in situ* neoantigens and adjuvants to LNs may be an effective approach to solve the abovementioned problems. Therefore, an FA-TSL/AuNCs/SV nanoplatfrom was constructed by integrating simvastatin (SV) adjuvant loaded Au nanocages (AuNCs) as cores (AuNCs/SV) and folic acid modified thermal-sensitive liposomes (FA-TSL) as shells to enhance *de novo* antitumor immunity. After accumulation in tumor guided by FA, AuNCs mediated photothermal therapy (PTT) induced the release of tumor-derived protein antigens (TDPAs) and the shedding of FA-TSL. Exposed AuNCs/SV soon captured TDPAs to form *in situ* recombinant vaccine (AuNCs/SV/TDPAs). Subsequently, AuNCs/SV/TDPAs could efficiently transport to draining LNs owing to the hyperthermia induced vasodilation effect and small particle size, achieving co-delivery of antigens and adjuvant for initiation of specific T cell response. In melanoma bearing mice, FA-TSL/AuNCs/SV and laser irradiation effectively ablated primary tumor, against metastatic tumors and induced immunological

*Corresponding authors.

E-mail addresses: fengqianhua@zzu.edu.cn (Qianhua Feng), wanglei1@zzu.edu.cn (Lei Wang).

†These authors made equal contributions to this work.

Peer review under responsibility of Chinese Pharmaceutical Association and Institute of Materia Medica, Chinese Academy of Medical Sciences.

<https://doi.org/10.1016/j.apsb.2022.02.026>

2211-3835 © 2022 Chinese Pharmaceutical Association and Institute of Materia Medica, Chinese Academy of Medical Sciences. Production and hosting by Elsevier B.V. This is an open access article under the CC BY-NC-ND license (<http://creativecommons.org/licenses/by-nc-nd/4.0/>).

memory. This approach served a hyperthermia enhanced platform drainage to enable robust personalized cancer vaccination.

© 2022 Chinese Pharmaceutical Association and Institute of Materia Medica, Chinese Academy of Medical Sciences. Production and hosting by Elsevier B.V. This is an open access article under the CC BY-NC-ND license (<http://creativecommons.org/licenses/by-nc-nd/4.0/>).

1. Introduction

Vaccines have protected countless people from various diseases and recently made some achievements in the fight against cancer^{1,2}. Despite taking a number of efforts to develop cancer vaccines, efficacious therapies still remain challenging due to high heterogeneity of tumor immunogenicity^{3,4}. In recent years, personalized vaccines targeting cancer-specific neoantigens have proposed to elicit individual antitumor immunity^{5,6}. However, the effectiveness of personalized vaccines is limited by various hurdles, such as costly and time-consuming acquirement process of neoantigens, low immunogenicity of single neoantigen peptides, rapid clearance of free neoantigens, as well as insufficient transport of antigens and adjuvants to lymph nodes (LNs)^{7–10}. Herein, it is urgent to develop a versatile vaccination strategy that can synergistically modulate multiple aspects for enhancing antitumor immunity.

LNs are the critical therapeutic target for various vaccines, which contain a large number of immature dendritic cells (DCs) presenting neoantigens to initiate strong T cell responses for adaptive immunity initiation^{11,12}. Peptide and protein antigens are broadly applied in cancer vaccines due to excellent immune activation effect as well as lower toxicity^{13,14}. However, neoantigen proteins/peptides are always cleared which result in low immunogenicity, further limiting optimal antigen presentation^{15–17}. Encouragingly, nano-engineering vaccines have been designed to overcome this obstacle. More interestingly, these nano-vaccines with an intermediate size (20–70 nm) prefer to drain to LNs and retain here^{18–20}. Therefore, vesicles with appropriate physical-biochemical properties are good candidates for vaccines construction.

A myriad of Au nanomaterials exhibits outstanding light-to-heat conversion efficiency due to the localized surface plasmon resonance, making them great potentials for cancer photothermal therapy (PTT)^{21–23}. Interestingly, PTT not only achieved tumor ablation *via* hyperthermia effect, but also enhanced nanodrugs accumulation in tumor site as well as antitumor immunity^{24,25}. Among various Au nanomaterials, AuNCs with particle size of 40–100 nm could induce the release of tumor-derived protein antigens (TDPAs), such as damage-associated molecular patterns (DAMPs) and neoantigens^{26,27}. It is noteworthy that Au nanomaterials with special surface can directly capture proteins through some forces such as Au–S bond, electrostatic interactions and hydrophobic interactions^{28,29}. So, AuNCs could not only convert cancer into a nidus for presentation of cancer antigens, but also capture these TDPAs to construct an *in situ* recombinant vaccine. Interestingly, negative surface and suitable particle size endow AuNCs based vaccine with excellent LNs drainage ability which could be further promoted by vasodilation effect under hyperthermia^{30,31}. This approach could avoid complicated preparation process and promote LNs drainage of personalized vaccine.

In addition to the above advantages, AuNCs with hollow mesoporous structure are in favour of the encapsulation of adjuvant that is essential to enhance antitumor immune responses²². It has been

reported that simvastatin (SV) exhibited vaccine adjuvant activities by blocking mevalonate (MVA) pathway. SV can arrest endosomal maturation, prolong antigen preservation during endocytosis, increase antigen presentation to both CD4⁺ and CD8⁺ T cells, thus displaying excellent immune-boosting effects³². Therefore, we are encouraged to encapsulate SV into AuNCs (AuNCs/SV) for the construction of *in situ* personalized cancer vaccine.

In light of these considerations, a folic acid modified thermal-sensitive liposomes (FA-TSL) shell was engineered onto the surface of AuNCs/SV to construct an FA-TSL/AuNCs/SV nanoplatform for *de novo* antitumor immunity (Fig. 1). FA-TSL shells could protect AuNCs/SV from interference of non-tumor-related proteins in circulation and guide the nanoplatform to tumor. After irradiation with 808 nm laser in tumor site, AuNCs mediated photothermal therapy (PTT) induce the release of TDPAs and the shedding of FA-TSL. Immediately, exposed AuNCs/SV capture TDPAs to form *in situ* recombinant vaccine (AuNCs/SV/TDPAs), which could efficiently transport to draining LNs due to hyperthermia induced vasodilation effect, negatively charged surface and appropriate particle size. Once in contact with DCs, the recombinant vaccine facilitated cross presentation of TDPAs to stimulate antitumor immune responses. This nanoplatform seeks to convert irradiated tumor into a nidus for presentation of TDPAs and transport these TDPAs to LNs, thus facilitating personalized *de novo* antitumor immunity.

2. Materials and methods

2.1. Materials

Silver nitrate (AgNO₃), sodium borohydride (NaBH₄) and trisodium citrate dihydrate (C₆H₅Na₃O₇·2H₂O) were obtained from Shanghai Sinopharm Chemical Reagent Co., Ltd. (China). Polyvinylpyrrolidone (PVP), 3-(4,5-dimethyl-2-thiazolyl)-2,5-diphenyl-2-*H*-tetrazolium bromide (MTT), hydrogen tetrachloroaurate tetrahydrate (HAuCl₄·4H₂O) and ovalbumin (OVA) were purchased from Sigma–Aldrich (St. Louis, MO, USA). Cholesterol and 1,2-dipalmitoyl-*sn*-glycero-3-phosphocholine (DPPC, 99.0%) were got from CordentPharma (Plankstadt, Germany). Polyethylene glycol-conjugated 1,2-distearoyl-*sn*-glycero-3-phosphoethanolamine-folic acid (DSPE-PEG2000-FA) was obtained from Shanghai Ponsure Biotech, Inc. (Shanghai, China). Fluorescein 5 (6)-isothiocyanate (FITC) was purchased from Aladdin (Shanghai, China). Cy5 dye was got from Beijing Solebo Technology Co., Ltd. (Beijing, China). All the other chemical reagents were obtained from Sigma–Aldrich. Anti-CD40-PE, anti-CD86-APC-R700, anti-CD45-APC-Cy7, anti-CD8a-PerCP-Cy5.5, anti-CD3-BV510 and anti-CD4-PE were purchased from BD biosciences (New Jersey, USA). Anti-CD11c-BV605, anti-CD44-PE, anti-CD62L-APC, anti-SIINFEKL-MHC-I-APC-R700 and anti-MHC-II-PE were purchased from BioLegend (CA, USA).

The mice melanoma B16F10 cell line in this study was from the China Center for Type Culture Collection at Wuhan University

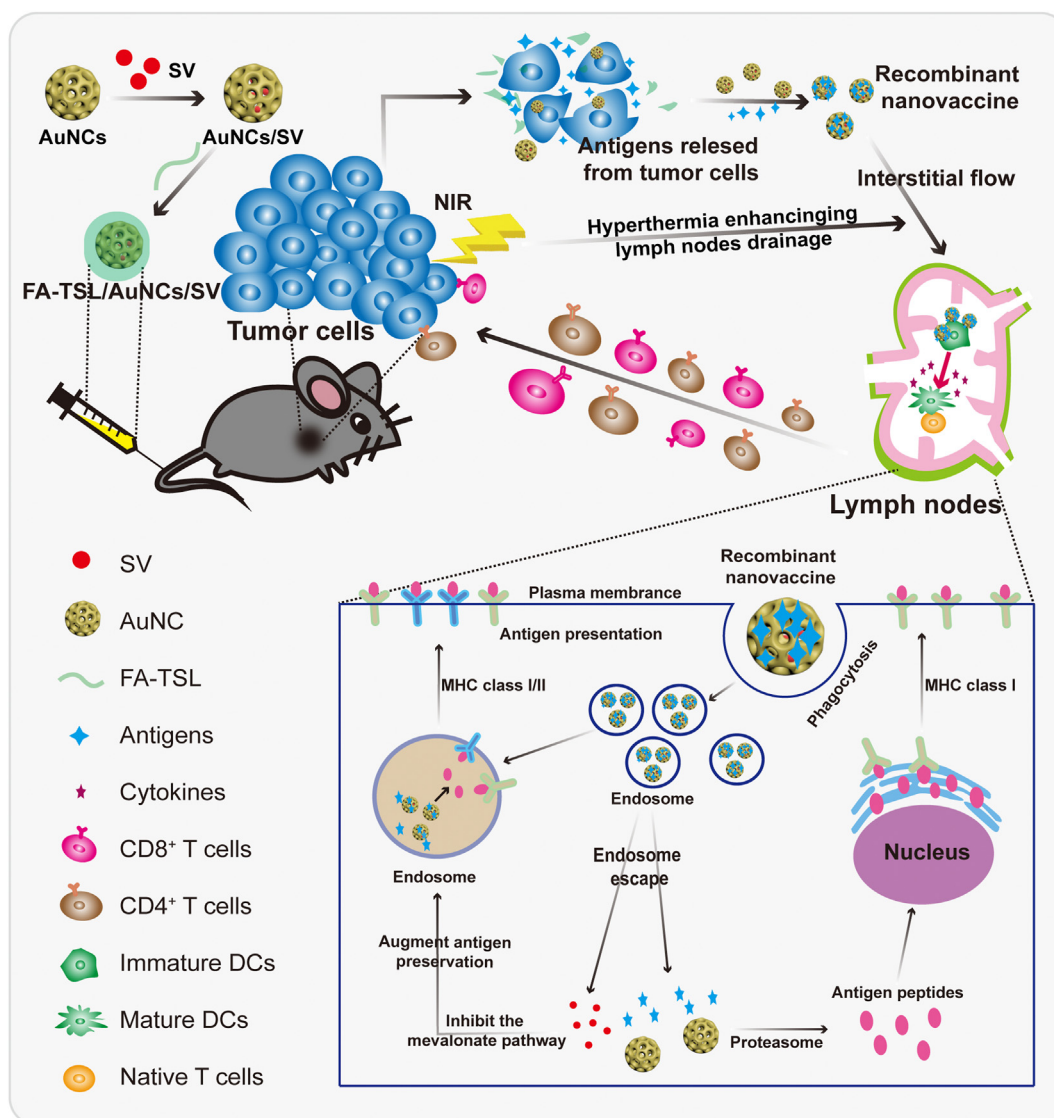


Figure 1 Schematic diagram of FA-TSL/AuNCs/SV with assistance of 808 nm laser to improve cancer immunotherapy.

(Hubei, China). B16F10 cells were incubated in RPMI 1640 medium supplemented with 10% fetal bovine serum (FBS), penicillin (100 units/mL) and streptomycin (100 $\mu\text{g}/\text{mL}$) in 5% CO_2 at 37 $^\circ\text{C}$. DCs were isolated from the C57BL/6J mice bone marrow.

Female C57BL/6J mice (six weeks old) were purchased from Center for Experimental Animals, Henan University. All animal studies were conducted in accordance with the guidelines of the National Regulation of China for Care and Use of Laboratory Animals.

2.2. Synthesis of AuNCs

28.5 nm silver nanoparticles (AgNPs) were prepared according to a previous report³³. Then, the 28.5 nm AgNPs were added into PVP solution that had been pre-stirred and heated at 90 $^\circ\text{C}$ for 1 h. After heating for 2 min, 0.1 mmol/L $\text{HAuCl}_4 \cdot 4\text{H}_2\text{O}$ solution was added at 0.7 mL per minute, and a series of color change could be observed^{34,35}. When the solution turned blue, addition of $\text{HAuCl}_4 \cdot 4\text{H}_2\text{O}$ solution was stopped. When color of mixed

solution was no longer changed, the reaction system was stopped and cooled down to room temperature. Then, AuNCs were collected and stored at 4 $^\circ\text{C}$ for further use.

2.3. Synthesis of FA-TSL/AuNCs/SV

To prepare AuNCs/SV NPs, SV (2 mg/mL) in methanol solution was mixed with AuNCs (2 mg/mL) in aqueous solution (2:1, v/v) and kept stirring for 24 h. Then, the mixture was centrifuged (12,000 rpm, 5 min, TGL-16G, Shanghai Anting Scientific Instrument Factory, Shanghai, China) and washed three times with deionized water/methanol (1:1, v/v) to remove free SV. AuNCs/SV were collected and re-dispersed in deionized water.

Subsequently, FA-TSL/AuNCs/SV were prepared by thin-film hydration method. Briefly, DPPC, cholesterol, DSPE-PEG2000-FA (7:1:0.5, mol/mol) were dissolved in chloroform³⁶. A lipid film was formed when chloroform was removed by using a rotary evaporator (RE-52AA, Shanghai, China). Next, AuNCs/SV solution was added to hydrate the film by gently rotating for 1 h. After sonication (200 W, 3/5 s on/off) for 3 min with a cell ultrasonic

pulverizer (JY 92-IIDN, Xinzhi Biological Technology Co., Ltd., Ningbo, China), the final FA-TSL/AuNCs/SV were prepared.

2.4. Characterization of FA-TSL/AuNCs/SV

FA-TSL/AuNCs/SV were characterized by dynamic light scattering (DLS) analyzer (Zetaster, Malvern, UK), transmission electron microscopy (TEM, JEOL, Japan), ultraviolet–visible (UV–Vis) spectrum (UV-2550, Shimadzu, Japan) and energy-dispersive spectroscopy (EDS) analysis (Oxford X-Max, Oxford Instruments, UK). Photothermal property of FA-TSL/AuNCs/SV was assessed by using 808 nm laser (Changchun new industry photoelectric technology Co., Ltd., Changchun, China). The temperature was monitored by infrared temperature instrument (Fluke Ti200, USA) at a 30 s interval.

2.5. Tumor antigens capture *in vitro*

FA-TSL/AuNCs/SV-containing medium was used to culture B16F10 cells and replaced with fresh RPMI 1640 after 4 h. Followed irradiation tumor cells with 808 nm laser (1.5 W/cm^2) for 2 min. After 20 h incubation, the cell supernatant was collected. Subsequently, insoluble cellular debris were removed by centrifugation of 2000 rpm for 5 min (TGL-16G, Shanghai Anting Scientific Instrument Factory). Then, AuNCs/SV/TDPAs were obtained from supernatant after centrifugation of 8000 rpm for 10 min (TGL-16G, Shanghai Anting Scientific Instrument Factory). The captured protein was characterized by sodium dodecyl sulfate polyacrylamide gel electrophoresis (SDS-PAGE), mass spectrometry and western blotting.

2.6. *In vitro* cytotoxicity of FA-TSL/AuNCs/SV

After incubation with FA-TSL/AuNCs/SV NPs for 4 h, B16F10 cells were irradiated with 808 nm laser (1.5 W/cm^2) for 2 min. After further culture for 20 h, cell viability and apoptosis were tested by MTT method and Calcein-AM/propidium iodide (calcein-AM/PI) (Yeasen Biotech Co., Ltd., Shanghai, China), respectively.

2.7. DCs uptake and lysosomal escape

Bone-marrow-derived dendritic cells (BMDCs) were incubated with FITC-labeled model antigens ovalbumin (FITC-OVA) and antigens-NPs (AuNCs/SV/FITC-OVA). Then cells uptake and prolonged antigen preservation were analyzed by flow cytometry and confocal laser scanning microscope (CLSM, Leica TCS SP8, Germany) respectively.

BMDCs were incubated different formulations similarly by uptake method to investigate lysosome escape. At 2 and 8 h, cells were collected and analyzed by CLSM (Leica TCS SP8, Germany), respectively. In addition, the expression of Rab5 and Rab7a in BMDCs were detected to investigate endosomal maturation.

2.8. Immune response examination *in vitro*

For immunogenic cell death (ICD) detection, B16F10 cells were treated with different formulations. Then, cells were collected to detect calreticulin (CRT) exposure by using anti-CRT-FITC antibody. Cell culture supernatant was collected to examine released intracellular high mobility group box 1 (HMGB1).

For DCs maturation measurement, BMDCs were incubated with antigens-NPs which were separated from NPs-containing cell lysate. 24 h later, DCs were marked with anti-CD86-FITC and anti-CD80-APC antibodies and analyzed by flow cytometry (Accuri C6, BD, USA).

2.9. *In vivo* distribution

Because fluorescence signals in tumor site of C57BL/6 mice were invisibility, BALB/c mice (female, 6–8 weeks) were used to detect *in vivo* biodistribution of the nanopatform. 4T1-bearing mice were intravenous injection (i.v.) injected with IR780-labeled FA-TSL and FA-TSL/AuNCs, respectively. IR780 signal was acquired by an IVIS spectrum *in vivo* imaging system (IVIS, PerkinElmer, USA) at scheduled time points.

2.10. *In vivo* antitumor activity

B16F10 tumor-bearing C57BL/6 mice were unconsciously divided into six groups ($n = 6$). Mice were i.v. injected with PBS, SV, FA-TSL/AuNCs, FA-TSL/AuNCs + laser, FA-TSL/AuNCs/SV and FA-TSL/AuNCs/SV + laser every 2 days for five times. Mice received different formulations at SV dose of 0.625 mg/kg and AuNCs dose of 0.625 mg/kg (Au concentration). The irradiation groups were irradiated with 808 nm laser (0.75 W/cm^2 , 3 min) at 4 h post injection. Tumor size and body weight were recorded during treatment. Tumor size was calculated according to the following Eq. (1):

$$\text{Volume} = \text{Length} \times \text{Width}^2/2 \quad (1)$$

Then, main organs were collected from sacrificed mice for hematoxylin and eosin (H&E) staining. Tumors were removed for H&E, terminal deoxynucleotidyl transferase dUTP nick-end labeling (TUNEL), CRT and HMGB1 staining.

2.11. Antitumor immunity

B16F10 tumor-bearing mice were i.v. administered different formulations to investigate antitumor immunity. Tumor, LNs and spleens were harvested and digested to single-cell suspension, which was stained with fluorescent-labeled antibody. Flow cytometry (BD FACS Canto, USA) was used to detect the percentage of matured DCs ($\text{CD45}^+\text{CD11c}^+\text{CD40}^+\text{CD86}^+$) and T cells ($\text{CD45}^+\text{CD3}^+\text{CD4}^+\text{CD8}^+$) in tumors, matured DCs, T cells, MHC I ($\text{CD45}^+\text{CD11c}^+\text{SIINFEKL-MHC-I}^+$) and MHC II ($\text{CD45}^+\text{CD11c}^+\text{MHC II}^+$) in LNs, and effector memory T cells (T_{EM}) cells ($\text{CD45}^+\text{CD3}^+\text{CD8}^+\text{CD44}^+\text{CD62L}^-$) in spleen. IFN- γ , TNF- α and IL-6 cytokines in serum were detected by ELISA kits (Multi-Sciences Biotech, China).

2.12. Abscopal effect

To study abscopal effect, B16F10 cells were (1×10^6 cells per side) subcutaneously injected in right flank of C57BL/6J mice on Day 0 (primary tumors) and left flank on Day 5 (secondary tumors). When the right tumor reached $\sim 100 \text{ mm}^3$, the mice were treated with drugs similar to those *in vivo*.

2.13. Investigation of lung metastasis

Anti-metastasis effectiveness of nanoplatform was investigated in a lung metastasis models. B16F10 cells were *i.v.* injected into C57BL/6 mice which received various treatments. On Day 21, whole lungs were excised and stained with H&E for quantification of metastasis area.

2.14. Statistical analysis

The data were presented as the mean \pm standard deviation (SD). All statistical analysis were processed with Graph Pad Prism 8.0 (La Jolla, CA, USA). The differences between two groups and multiple groups were analyzed by one-way ANOVA and two-way ANOVA, respectively. The level of significance was set at probabilities: * $P < 0.05$, ** $P < 0.01$, *** $P < 0.001$.

3. Results and discussion

3.1. Synthesis and characterization of FA-TSL/AuNCs/SV

AuNCs were prepared by employing Ag NPs as the sacrificial templates^{37,38}. TEM results indicated that AuNCs with average diameter of ~ 40 nm showed hollow mesoporous structure (Fig. 2A). Moreover, elemental mapping (Fig. 2B) and EDS (Fig. 2C) analysis demonstrated the presence of Au element. The diffraction pattern in Fig. 2D showed the peaks appeared at 38.3° , 44.5° , 64.7° , 77.7° and 82.3° , which were assigned to crystalline planes of gold nanostructure (JCPDS 04-0874), indicating the existence of gold crystalline phases³⁹. After encapsulation of SV, AuNCs/SV showed no obvious difference in particle size (Supporting Information Fig. S1A), zeta potential (Fig. S1B) and morphology (Supporting Information Fig. 2E). A distinct absorption peak at ~ 240 nm was observed in UV–Vis spectrum of AuNCs/SV (Supporting Information Fig. S2), demonstrating successful loading of SV. Afterward, FA-TSL was coated onto AuNCs/SV surface to obtain FA-TSL/AuNCs/SV. DLS displayed a particle size of 55.3 ± 0.80 nm and a zeta potential of -18.9 ± 0.79 mV for FA-TSL/AuNCs/SV (Fig. S1). Then, the existence of FA-TSL was further confirmed by TEM (Fig. 2F), which revealed an obvious core–shell structure. Above results validated the construction of FA-TSL/AuNCs/SV.

Then, FA-TSL/AuNCs/SV were resuspended in 1640 medium containing 10% fetal bovine serums to test the stability. As indicated in Supporting Information Fig. S3, particle size and morphology had no obvious change after 14 days incubation, suggesting that FA-TSL could protect AuNCs/SV from capturing non-tumor-related proteins in circulation. Subsequently, the photothermal property of FA-TSL/AuNCs/SV was studied. As shown in Fig. 2G, both AuNCs and FA-TSL/AuNCs/SV experienced rapid temperature increase under 808 nm laser irradiation (1.5 W/cm^2), while no obvious temperature change was detected in control group. Additionally, FA-TSL/AuNCs/SV showed an Au dose and time dependent manner in temperature increasement research (Supporting Information Fig. S4). Moreover, FA-TSL/AuNCs/SV exhibited no obvious attenuation of maximum solution temperature during four cycles of laser irradiation (Supporting Information Fig. S5), demonstrating their remarkable photostability. After treatment with laser irradiation, the size and zeta potential were changed obviously and in line with that of AuNCs/SV (Supporting Information Fig. S6). In addition,

FA-TSL/AuNCs/SV exhibited spherical core–shell structure, while naked AuNCs/SV were observed by TEM (Fig. 2H). Above results suggested the shedding of FA-TSL, which is necessary for AuNCs/SV exposure and antigen absorption.

3.2. Construction of recombinant vaccine

B16F10 melanoma cells were incubated with FA-TSL/AuNCs/SV and treated with 808 nm laser irradiation for *in vitro* recombinant vaccine construction (Fig. 2I). As shown in Fig. 2J, a TDPAs layer could be obviously observed on the surface of AuNCs. Then, the total amount of absorbed antigens was quantified using bicinchoninic acid (BCA) assay, which showed significant Au concentration-dependence (Fig. 2K). Moreover, TDPAs were quite different from raw cell lysate of untreated B16F10 cells, as SDS-PAGE indicated (Fig. 2L). To determine whether AuNCs/SV captured proteins contained neoantigens expressed by B16F10 cells, proteins types of TDPAs were identified by using mass spectrometry. As Fig. 2M displayed, the recombinant vaccine contained neoantigens and DAMPs. In addition, tumor specific antigens, such as ACTN4, TNPO3, GP100 and MAK23, were further determined by western blotting (Fig. 2N). The above results demonstrated that TDPAs produced by tumor cells during hyperthermia therapy could be used to construct recombinant vaccine for specific antitumor immunotherapy.

3.3. Cells experiments on B16F10

Cellular uptake experiment was next investigated in B16F10 cells. Fig. 3A and Supporting Information Fig. S7 showed that FA-TSL/AuNCs/FITC could be engulfed by tumor cells more effectively than that of FITC and TSL/AuNCs/FITC, which was mainly due to FA receptor-mediated endocytosis. Then, standard MTT assay was used to investigate cytotoxicity of different formulations. As shown in Fig. 3B, all preparations showed no obvious cytotoxicity without laser irradiation. However, FA-TSL/AuNCs/SV resulted in $\sim 90\%$ cell death at an Au dose of $50 \mu\text{g/mL}$ (Fig. 3C), which was further confirmed by high proportion of PI positive cells (Fig. 3D).

Several studies have demonstrated that PTT can elicit ICD by inducing dying tumor cells to expose CRT and release HMGB1^{40–42}. Then, the CRT exposure of treated B16-F10 tumor cells was evaluated. As shown in Fig. 3E, FA-TSL/AuNCs/SV with 808 nm laser treatment obviously enhanced CRT exposure. Similarly, FA-TSL/AuNCs/SV and laser irradiation induced the highest level of HMGB1 release, as displayed in Fig. 3F. All these results demonstrated that FA-TSL/AuNCs/SV with 808 nm laser induced PTT could kill tumor cells and induce ICD effect.

3.4. Uptake and activation of BMDCs

Subsequently, FITC-labeled ovalbumin (FITC-OVA) was used as the model antigen to investigate mechanism of DCs maturation promoted by recombinant vaccine. Firstly, the internalization of FITC-OVA and AuNCs/SV/FITC-OVA by BMDCs was examined, respectively. According to Supporting Information Fig. S8 fluorescence intensity in AuNCs/SV/FITC-OVA group gradually increased with extended time and reached highest level at 8 h, which was significantly stronger than that in FITC-OVA group (Fig. 3G). Next, intracellular fate of AuNCs/SV/FITC-OVA was evaluated using CLSM. The result in Fig. 3H indicated that lysosomes signal (red) and NPs signal (green) completely overlapped after 4 h incubation. With the extension of incubation time,

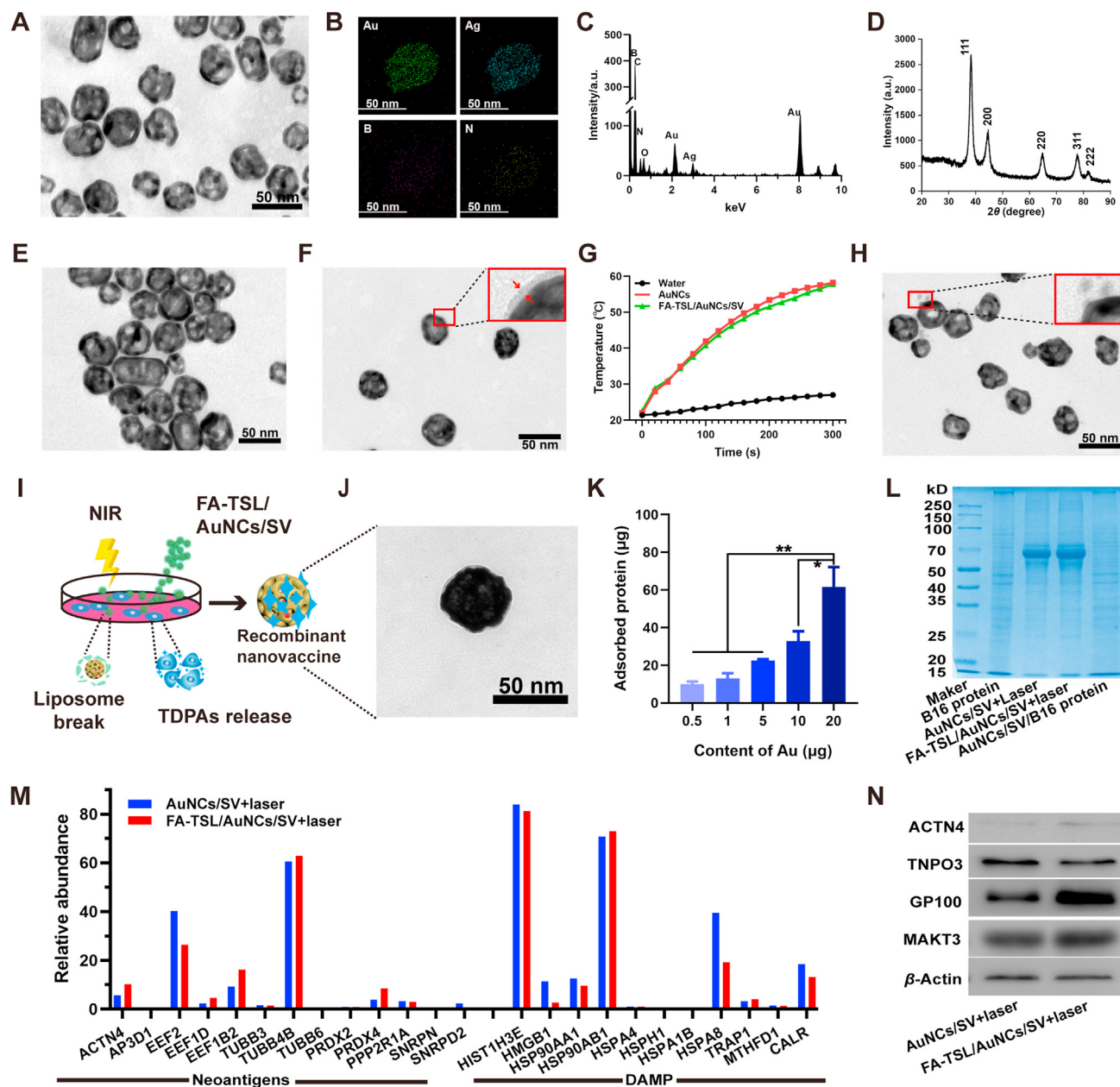


Figure 2 (A) TEM image of AuNCs. (B) Elemental mapping of AuNCs. (C) EDS analysis of AuNCs. (D) X-ray diffraction (XRD) of AuNCs. (E) TEM image of AuNCs/SV. (F) TEM image of FA-TSL/AuNCs/SV. (G) Photothermal activity of AuNCs and FA-TSL/AuNCs/SV with Au concentration of 50 $\mu\text{g}/\text{mL}$ under 1.5 W/cm^2 of 808 nm laser. (H) TEM image of FA-TSL/AuNCs/SV + laser. (I) Schematic diagram of the preparation of *in vitro* recombinant vaccine. (J) TEM image of AuNCs/SV/TDPAs. (K) Total amount of captured antigens by AuNCs/SV. (L) SDS-PAGE analysis of B16 proteins and AuNCs/SV binding proteins. (M) The relative abundance of neoantigens and DAMPs captured by NPs in AuNCs/SV + laser and FA-TSL/AuNCs/SV + laser groups. The data are presented as mean \pm SD ($n = 3$). * $P < 0.05$, ** $P < 0.01$.

green fluorescence was overflowed from red lysotracker at 8 h, indicating that these NPs escaped from endo/lysosomes, which was important for SV to exert its adjuvant effect. It is well known that Rab5 expressed early endosomes mature through acidification and material exchange to form Rab7a expressed late endosomes^{43,44}. After treatment with AuNCs/TDPAs and AuNCs/SV/TDPAs, the expression of Rab5 and Rab7a were observed by CLSM. As displayed in Supporting Information Fig. S9, the transition from an Rab5-positive to an Rab7a-positive endosome was significantly slowed down by AuNCs/SV/TDPAs. Meanwhile,

AuNCs/SV/TDPAs treatment dramatically increased the retention time of model antigen OVA in BMDCs (Supporting Information Fig. S10), which was meaningful for antigen presentation and immune activation.

To verify immune response activation, the effects of AuNCs/SV/TDPAs and other formulations on BMDCs maturation were further studied. After different treatments, flow cytometry was used to quantify the frequency of DCs maturation. As shown in Fig. 3I and Supporting Information Fig. S11, TDPAs, SV, AuNCs, AuNCs/TDPAs, AuNCs/SV and AuNCs/SV/TDPAs groups

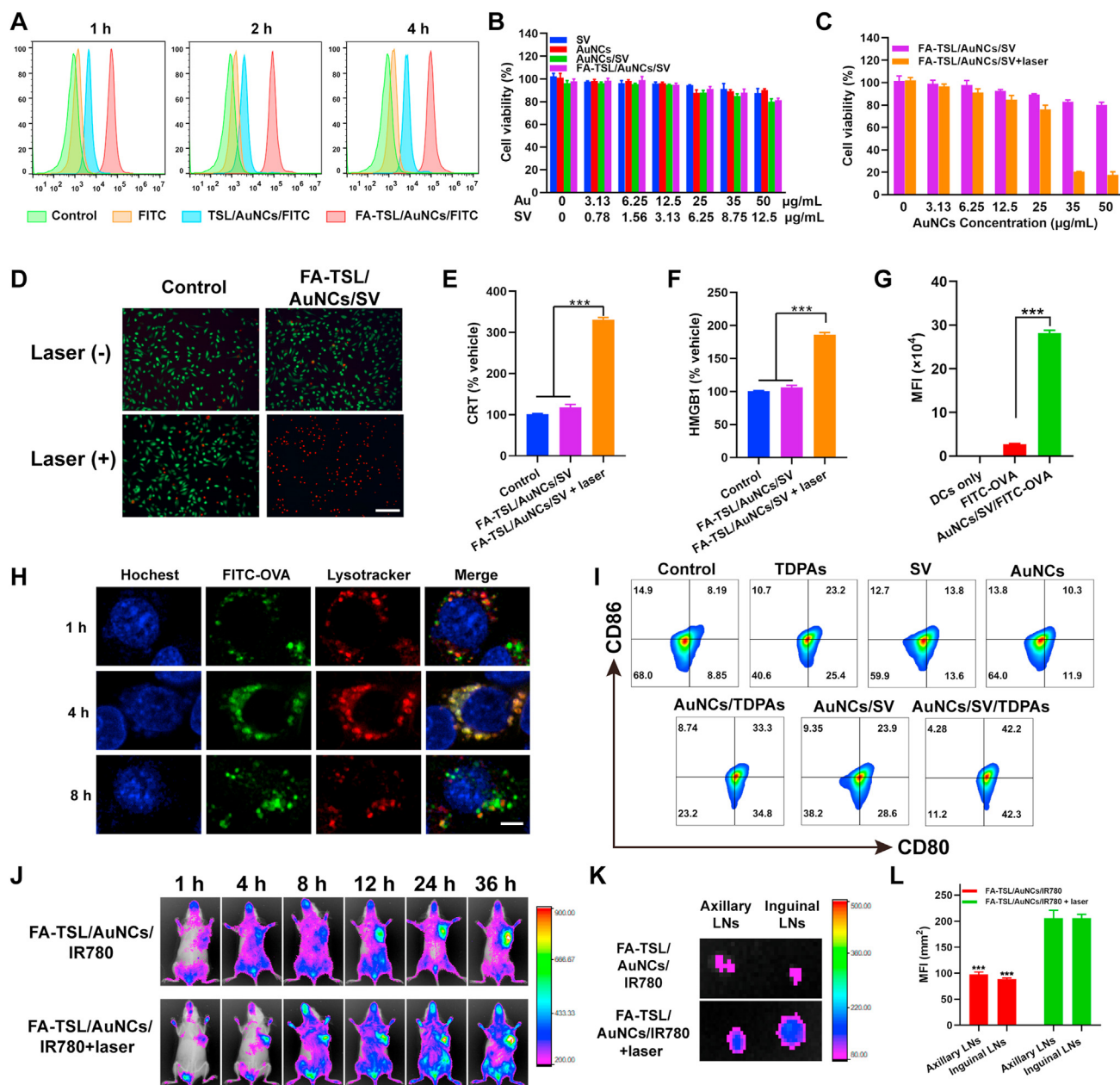


Figure 3 (A) Cellular uptake (scale bar = 100 μm). (B) Cytotoxicity of B16F10 cells. (C) Cytotoxicity of B16F10 cells with 808 nm laser irradiation (1.5 W/cm², 2 min). (D) Calcein-AM/PI staining (scale bar = 100 μm). (E) Surface CRT expression. (F) Extracellular release of HMGB1. (G) The quantitative analysis of DCs uptake of FITC-OVA. (H) Lysosomal escape test (scale bar = 10 μm). (I) DCs maturation measurement. (J) FRI of mice received different formulations. (K) FRI of LNs harvested from mice at 36 h. (L) Quantification of fluorescence intensity in axillary and inguinal LNs. The results of significant difference analysis were compared with FA-TSL/AuNCs/IR780 + laser group. The data are presented as mean ± SD ($n = 3$). *** $P < 0.001$.

exhibited around 23.62%, 13.40%, 10.87%, 33.55%, 23.82% and 41.85% of DCs maturation, respectively. Therefore, the recombinant vaccine was able to bring out an enhanced immunotherapy by boosting immune response.

3.5. Tumor targeting and LNs drainage ability assessment

Afterward, IR780-labeled nanoplateform was used to investigate tumor targeting and LNs drainage ability of FA-TSL/AuNCs/SV. In detail, FA-TSL/AuNCs/IR780 were administrated by i.v., and then their biodistribution *in vivo* was detected by a near-infrared

fluorescence imaging system. The experimental results in Supporting Information Fig. S12 revealed that IR780 fluorescence showed effective accumulation in tumors after injection of FA-TSL/AuNCs/IR780 compared with free IR780, demonstrating good tumor-targeting effect of this nanoplateform. Next, LNs migration ability of recombinant vaccine was also evaluated. The results of fluorescence reflectance imaging (FRI, Fig. 3J) showed that more IR780-labeled nanoplateform transport to lymphatic system with assistance of 808 nm laser irradiation, which mainly attributed to small size of AuNCs and photothermal induced vasodilation effect^{45,46}. The axillary and inguinal draining LNs

were collected from sacrificed mice at 36 h. As displayed in Fig. 3K and L, the intensity of IR780 signal in axillary and inguinal LNs was significantly higher after treated with 808 nm laser.

To verify the drainage of recombinant vaccine *via* lymphatic vessels, FITC-labelled AuNCs were administrated by *i.v.* The tumor tissue was collected at 4 h post laser irradiation and stained with podoplanin which is expressed specifically in lymphatic endothelium^{47,48}. As shown in Supporting Information Fig. S13, the green fluorescence of FITC could be clearly observed in lymphatic vessels. Moreover, large amounts of AuNCs/FITC accumulated around lymphatic vessels, further confirmed the lymphatic drainage pathway of the recombinant vaccines. All above results proved that FA-TSL/AuNCs/IR780 and laser irradiation could enhance LNs-drainage effect of the recombinant vaccine, which could further improve the antitumor immunotherapy.

3.6. *In vivo* antitumor effect induced by FA-TSL/AuNCs/SV + laser

To assess *in vivo* PTT and therapeutic efficacy of FA-TSL/AuNCs/SV, tumor-bearing mice model was constructed by subcutaneous injection of B16F10 cells into right axilla of C57BL/6J mice. The mice were injected with different preparations and irradiated with 808 nm (0.75 W/cm², 3 min) laser at 4 h post injection. Tumor thermal images were recorded by infrared (IR) thermal image instrument. After irradiation for 5 min, temperature-rise curves and IR images displayed that tumor temperature of the mice treated with FA-TSL/AuNCs/SV and laser irradiation reached to ~52.3 °C (Supporting Information Fig. S14). Such superior *in vivo* photothermal effect of FA-TSL/AuNCs/SV was ascribed to their enhanced tumor accumulation and high photothermal conversion efficiency.

Then, *in vivo* antitumor effect was evaluated and experiment schedule was designed in Fig. 4A. Tumor-bearing mice were unconsciously divided into six groups and treated with Saline (as control group), SV, FA-TSL/AuNCs, FA-TSL/AuNCs + laser, FA-TSL/AuNCs/SV, and FA-TSL/AuNCs/SV + laser. As shown in Fig. 4B, FA-TSL/AuNCs + laser treatment only slightly inhibited tumor growth in the absence of SV adjuvant, while FA-TSL/AuNCs/SV + laser could significantly delay tumor growth. After treatment with FA-TSL/AuNCs/SV + laser, 50% of the animals were still alive at 50 days, and two out of six were tumor free at the end of experiment (Fig. 4C). Efficient immune activation induced by co-delivery of TDPAs and SV might account for this phenomenon. Moreover, immunohistochemical and immunofluorescent examinations were used to analyze tumor tissues after various treatments (Fig. 4D). H&E-stained image significantly enlarged apoptosis or necrosis areas in tumor tissues after treatment with FA-TSL/AuNCs/SV + laser. TUNEL staining also proved the excellent anticancer effect of FA-TSL/AuNCs/SV complex with laser irradiation. In addition, all tumor-bearing mice did not show significant weight loss during treatments (Supporting Information Fig. S15). H&E staining showed that no inflammation or necrosis was observed in main organs of mice treated with different formulations and there were no significant differences in all groups (Supporting Information Fig. S16). Furthermore, safety profile of the formulations was evaluated by blood routine, liver function and kidney function examination. The parameters of hepatic and renal function including alanine aminotransferase (ALT), aspartate aminotransferase (AST), creatinine (CREA) and urea showed no significant difference between healthy and FA-TSL/AuNCs/SV treated mice.

Similarly, same phenomenon was observed in the detection of white blood cells (WBC), red blood cells (RBC), blood platelet (PLT) and hemoglobin (HGB) (Supporting Information Fig. S17). Thus, these data demonstrated the excellent tumor suppressive ability and good biocompatibility of FA-TSL/AuNCs/SV.

3.7. Antitumor immune responses

To further elucidate potential antitumor mechanism of FA-TSL/AuNCs/SV, mice immune status was subsequently analyzed by immunofluorescent examination and flow cytometry. As shown in Fig. 4E and F and Supporting Information Fig. S18, FA-TSL/AuNCs + laser and FA-TSL/AuNCs/SV + laser could significantly increase CRT expression and HMGB1 level in tumor tissue compared with un-irradiation groups, indicating that FA-TSL/AuNCs based PTT might significantly increase tumor immunogenicity by inducing tumor ICD.

DCs, as a kind of APCs, are key to innate and adaptive immunity. The maturation of DCs promoted the binding of major histocompatibility complex (MHC) peptide and T cell receptor (TCR) for T cell activation^{49–51}. The ability of FA-TSL/AuNCs/SV to recruit DCs *via* photothermal effect and activate DCs by delivered AuNCs/SV/TDPAs were estimated by measuring mature DCs (CD11c⁺CD40⁺CD80⁺) in tumor tissue. After treated with FA-TSL/AuNCs/SV + laser, the frequency of mature DCs increased from 8.23% to 62.96% compared to untreated group (Supporting Information Fig. S19A). DCs maturation ratio in FA-TSL/AuNCs/SV + laser group was around 1.8- and 3.9-fold compared to that of FA-TSL/AuNCs + laser and FA-TSL/AuNCs/SV groups respectively, suggesting that adjuvant was necessary for enhancement of antigen presentation³². Correspondingly, highest percentage of tumor-infiltrating cytotoxic T cell (CTLs) (CD3⁺CD8⁺) was observed in FA-TSL/AuNCs/SV + laser group (Fig. S19B), implying that FA-TSL/AuNCs/SV combined with laser irradiation strategy could evoke T cell-mediated antitumor immunity.

To verify systemic immune activation, tumor draining LNs and spleen were collected and analyzed by flow cytometry. According to Fig. 4G, CD40⁺CD86⁺ DCs population was only increased in FA-TSL/AuNCs/SV with laser irradiation treatment group. These results demonstrated that the absence of antigen or adjuvant could not induce efficient immune response, which was confirmed by low CD40⁺CD86⁺ frequency in FA-TSL/AuNCs/SV and FA-TSL/AuNCs + laser groups. A major function of SV adjuvant is promotion of antigen presentation, in which process MHC played a key role³². Flow cytometry results suggested that FA-TSL/AuNCs/SV + laser treatment could significantly increase CD11c⁺MHCI⁺ (12.03%) and CD11c⁺MHCII⁺ (7.49%) DCs populations (Fig. 4H and I). In contrast, relatively few MHC⁺ DCs populations were detected in FA-TSL/AuNCs group, further confirming that AuNCs/SV/TDPAs had major effect on antigen presentation and immune activation.

After antigen presentation, naive CD8⁺ and CD4⁺ T cells were activated and gained their cytotoxic capabilities and helper functions. As shown in Fig. 4J and K, FA-TSL/AuNCs/SV with 808 nm laser treatment increased the helper CD4⁺ and CTLs in LNs and the frequency of CD4⁺ and CD8⁺ T cells were 2.57- and 2.59-fold compared to control group respectively. Subsequently, long-term antitumor immune response was examined by testing memory T cells (T_{EM}) in spleen. FA-TSL/AuNCs/SV + laser group significantly increased T_{EM} frequency in spleen, whereas FA-TSL/AuNCs/SV and FA-TSL/AuNCs + laser showed moderate efficacy to generate T_{EM}

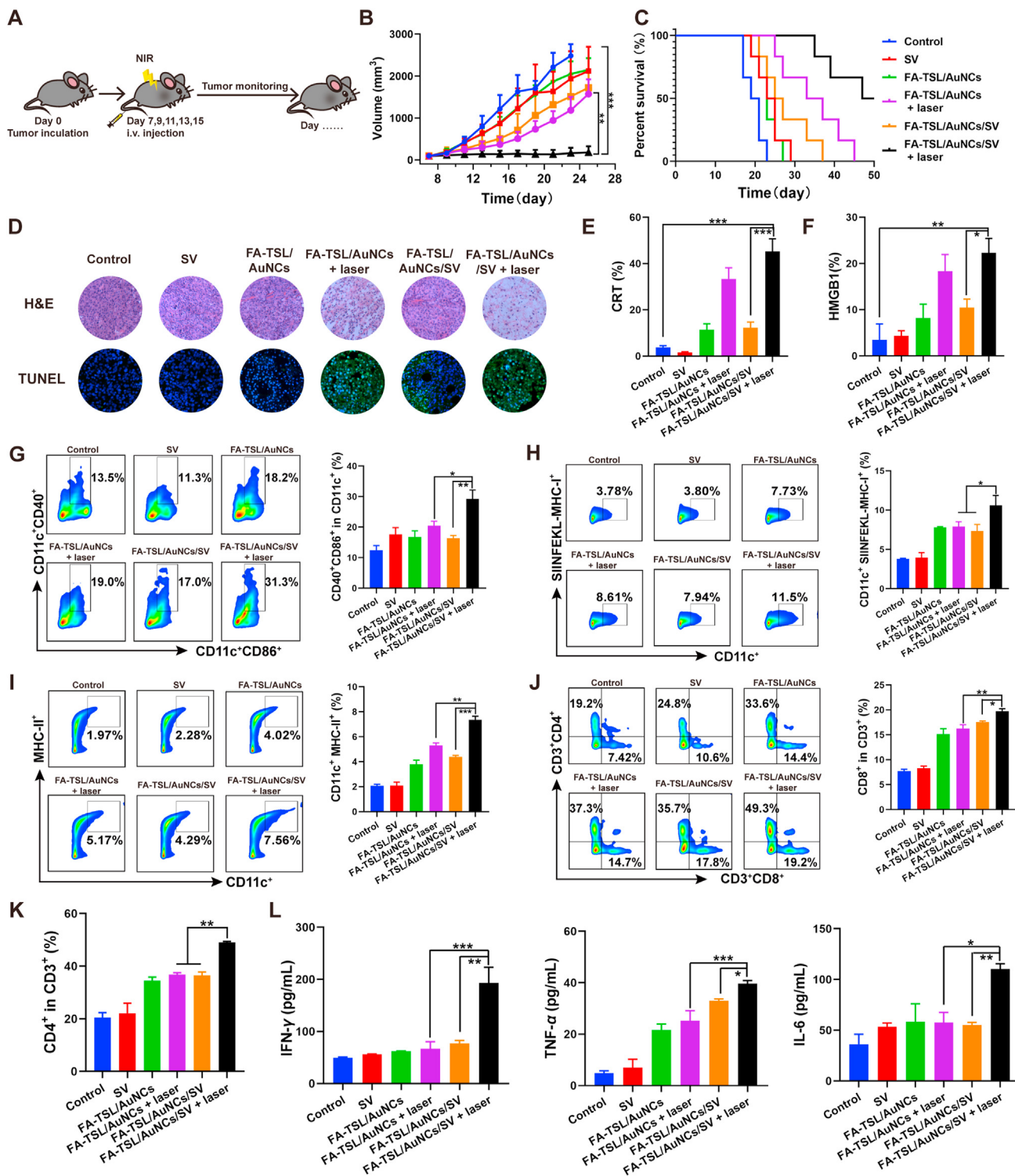


Figure 4 (A) Schematic illustration of experiment design. (B) *In vivo* tumor growth curve. (C) Mice survival curve. (D) H&E and TUNEL staining. (E) CRT expression in tumor tissue. (F) HMGB1 level in tumor tissue. The data are presented as mean \pm SD ($n = 6$). (G) Mature DCs in draining LNs. (H) MHC I molecules in draining LNs. (I) MHC II molecules in draining LNs. (J) CD3⁺ CD8⁺ T cells and (K) CD3⁺ CD4⁺ T cells in draining LNs. (L) Cytokine levels of IL-6, TNF- α , IFN- γ in serum. The data are presented as mean \pm SD ($n = 3$). * $P < 0.05$, ** $P < 0.01$, *** $P < 0.001$.

(Supporting Information Fig. S20). Furthermore, we analyzed anti-tumor immunity cytokines with immune capabilities. As shown in Fig. 4L, compared with other groups, FA-TSL/AuNCs/SV + laser

group expressed highest level of interleukin-6 (IL-6), tumor necrosis factor- α (TNF- α) and interferon- γ (IFN- γ) in serum. Collectively, these results suggested that PTT-mediated recombinant vaccine based

on AuNCs successfully induced a strong innate and adaptive immune response *in vivo*.

3.8. Abscopal effect and anti-metastasis evaluation

System antitumor immune response has been found to facilitate abscopal effect¹³. In order to further verify FA-TSL/AuNCs/SV with laser irradiation treatment induced antitumor immunity, we assessed abscopal effect of different treatments by measuring growth rate of the secondary tumors. A bilateral B16F10 subcutaneous tumor model was established and the schedule of animal experiments was revealed in Fig. 5A. Tumor in right axillary was

defined as a primary tumor and distant tumor was in left axillary. As presented in Fig. 5B–D, FA-TSL/AuNCs/SV with laser irradiation treatment could significantly suppress primary tumors and distant tumor compared with other groups. Moreover, there was no significant change in body weight (Fig. 5E). In addition, FA-TSL/AuNCs/SV with laser irradiation treatment had a 100% survival rate for 30 days and 40% for 50 days (Fig. 5F), consistently confirming excellent antitumor efficacy of this therapy regimen. Simultaneously, we constructed a melanoma metastatic tumor model to study the anti-metastasis effect of different preparations (Fig. 5G). As shown in Fig. 5H, FA-TSL/AuNCs/SV with laser irradiation treatment had almost no metastatic nodules. On the

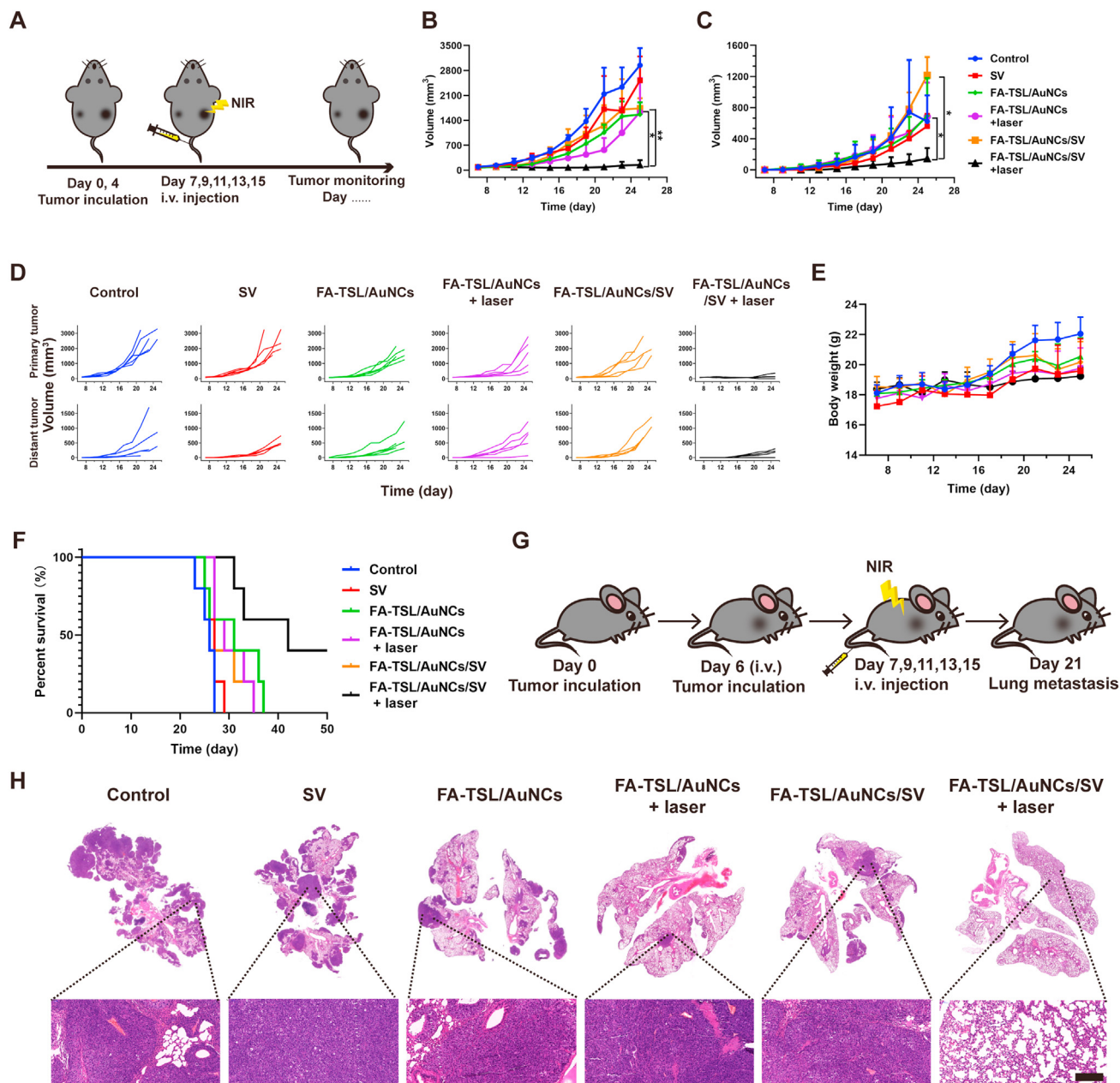


Figure 5 (A) Schematic illustration of the experiment design. (B) Primary tumor growth curves. (C) Distant tumor-growth curves. (D) Individual growth curves of primary and distant tumors. (E) Body weight. (F) Survival curve. The data are presented as mean \pm SD ($n = 6$). (G) Scheme for lung metastasis inhibition. (H) Representative H&E staining of lung tissue (scale bar = 200 μ m). The data are presented as mean \pm SD ($n = 3$). * $P < 0.05$, ** $P < 0.01$.

whole, the nano-system could inhibit both distant and metastatic tumor by activating systemic immune responses effectively.

4. Conclusions

In summary, this work first describes that a personalized *in situ* recombinant vaccine is drained to lymph nodes by hyperthermia to drive specific antitumor immunity. FA-TSL/AuNCs/SV + laser treatment turn tumors into a nidus of TDPAs to construct a recombinant antitumor vaccine *in vivo*. Impressively, the recombinant vaccine could efficiently flow into LNs owing to its particle size of ≈ 50 nm and the hyperthermia induced vasodilation effect. And it increased the number of mature DCs in tumor site and draining LNs due to the co-delivery and synergism of TDPAs and SV, resulting in the strong activation of CD4⁺ and CD8⁺ T cells. By using bilateral subcutaneous melanoma tumor model, our results indicated that FA-TSL/AuNCs/SV combined laser irradiation treatment induce a systemic immune response, resulting in delayed tumor growth of primary and distant, as well as prevented tumor metastasis. Potentially, this approach might offer a new strategy to induce robust personalized vaccination.

Acknowledgements

This project was financially supported by the National Natural Science Foundation of China (Grant Nos. U1804183, 81901878 and 81874304), China Postdoctoral Science Foundation (2019M662553, China) and Key Scientific Research Project (Education Department of Henan Province, 20HASTIT049, China).

Author contributions

Lei Wang and Qianhua Feng designed the research. Cuixia Zheng and Xinxin Liu carried out the experiments and performed data analysis. Yueyue Kong, Lei Zhang, Qingling Song, Hongjuan Zhao, Lu Han and Jiannan Jiao participated a part of the experiments. Lei Wang and Qianhua Feng provided experimental drugs and quality control. Cuixia Zheng and Xinxin Liu wrote the manuscript. Cuixia Zheng, Xinxin Liu and Yueyue Kong revised the manuscript. All of the authors have read and approved the final manuscript.

Conflicts of interest

The authors have no conflicts of interest to declare.

Appendix A. Supporting information

Supporting data to this article can be found online at <https://doi.org/10.1016/j.apsb.2022.02.026>.

References

- Saxena M, van der Burg SH, Melief CJM, Bhardwaj N. Therapeutic cancer vaccines. *Nat Rev Cancer* 2021;**21**:360–78.
- Banchereau J, Palucka K. Immunotherapy: cancer vaccines on the move. *Nat Rev Clin Oncol* 2018;**15**:9–10.
- Sahin U, Türeci Ö. Personalized vaccines for cancer immunotherapy. *Science* 2018;**359**:1355–60.
- Zhao H, Xu J, Li Y, Guan XX, Han X, Xu YY, et al. Nanoscale coordination polymer based nanovaccine for tumor immunotherapy. *ACS Nano* 2019;**13**:13127–35.
- Li AW, Sobral MC, Badrinath S, Choi Y, Graveline A, Stafford AG, et al. A facile approach to enhance antigen response for personalized cancer vaccination. *Nat Mater* 2018;**17**:528–34.
- Patel RB, Ye M, Carlson PM, Jaquish A, Zangl L, Ma B, et al. Development of an *in situ* cancer vaccine via combinational radiation and bacterial-membrane-coated nanoparticles. *Adv Mater* 2019;**31**:e1902626.
- Blass E, Ott PA. Advances in the development of personalized neoantigen-based therapeutic cancer vaccines. *Nat Rev Clin Oncol* 2021;**18**:215–29.
- Li WH, Li YM. Chemical strategies to boost cancer vaccines. *Chem Rev* 2020;**120**:11420–78.
- Yu X, Dai YF, Zhao YF, Qi SH, Liu L, Lu LS, et al. Melittin-lipid nanoparticles target to lymph nodes and elicit a systemic anti-tumor immune response. *Nat Commun* 2020;**11**:1110–3.
- Hong XY, Zhong XF, Du GS, Hou YY, Zhang YT, Zhang ZR, et al. The pore size of mesoporous silica nanoparticles regulates their antigen delivery efficiency. *Sci Adv* 2020;**6**:eaaz4462.
- Pulendran B, Ahmed R. Immunological mechanisms of vaccination. *Nat Immunol* 2011;**12**:509–17.
- Qian Y, Jin HL, Qiao S, Dai YF, Huang C, Lu LS, et al. Targeting dendritic cells in lymph node with an antigen peptide-based nanovaccine for cancer immunotherapy. *Biomaterials* 2016;**98**:171–83.
- Min Y, Roche KC, Tian S, Eblan MJ, McKinnon KP, Caster JM, et al. Antigen-capturing nanoparticles improve the abscopal effect and cancer immunotherapy. *Nat Nanotechnol* 2017;**12**:877–82.
- Zeng LM, Liao ZL, Li WW, Yuan QJ, Wu P, Gu ZP, et al. Non-covalent glycosylated gold nanoparticles/peptides nanovaccine as potential cancer vaccines. *Chin Chem Lett* 2020;**31**:1162–4.
- Kim Y, Kang S, Shin H, Kim T, Yu B, Kim J, et al. Sequential and timely combination of a cancer nanovaccine with immune checkpoint blockade effectively inhibits tumor growth and relapse. *Angew Chem Int Ed Engl* 2020;**59**:14628–38.
- Fan Y, Moon JJ. Nanoparticle drug delivery systems designed to improve cancer vaccines and immunotherapy. *Vaccines (Basel)* 2015;**3**:662–85.
- Zhao HJ, Zhao BB, Wu LX, Xiao HF, Ding KL, Zheng CX, et al. Amplified cancer immunotherapy of a surface-engineered antigenic microparticle vaccine by synergistically modulating tumor microenvironment. *ACS Nano* 2019;**13**:12553–66.
- Kim SY, Noh YW, Kang TH, Kim JE, Kim S, Um SH, et al. Synthetic vaccine nanoparticles target to lymph node triggering enhanced innate and adaptive antitumor immunity. *Biomaterials* 2017;**130**:56–66.
- Wang BH, An JY, Zhang HF, Zhang SD, Zhang HJ, Wang L, et al. Personalized cancer immunotherapy via transporting endogenous tumor antigens to lymph nodes mediated by nano Fe₃O₄. *Small* 2018;**14**:e1801372.
- Thomas SN, Vokali E, Lund AW, Hubbell JA, Swartz MA. Targeting the tumor-draining lymph node with adjuvanted nanoparticles reshapes the anti-tumor immune response. *Biomaterials* 2014;**35**:814–24.
- Zhang AM, Hai L, Wang TZ, Cheng H, Li M, He XX, et al. NIR-triggered drug delivery system based on phospholipid coated ordered mesoporous carbon for synergistic chemo-photothermal therapy of cancer cells. *Chin Chem Lett* 2020;**31**:3158–62.
- Huang SN, Duan SF, Wang J, Bao SJ, Qiu XJ, Li CM, et al. Folic-acid-mediated functionalized gold nanocages for targeted delivery of anti-miR-181b in combination of gene therapy and photothermal therapy against hepatocellular carcinoma. *Adv Funct Mater* 2016;**26**:2532–44.
- Hu YY, Lin L, Guo ZP, Chen J, Maruyama A, Tian HY, et al. *In situ* vaccination and gene-mediated PD-L1 blockade for enhanced tumor immunotherapy. *Chin Chem Lett* 2021;**32**:1770–4.
- Zhao XY, Han Y, Sun Y, Feng W, Liu JG, Li DS, et al. Combining photothermal ablation-based vaccine with immune checkpoint blockade for synergistic osteosarcoma immunotherapy. *Mater Design* 2021;**198**:190311.
- Yang SQ, Zhou LZ, Su Y, Zhang R, Dong CM. One-pot photoreduction to prepare NIR-absorbing plasmonic gold nanoparticles tethered by amphiphilic polypeptide copolymer for synergistic photothermal-chemotherapy. *Chin Chem Lett* 2019;**30**:187–91.

26. Chen JY, Glaus C, Laforest R, Zhang Q, Yang MX, Gidding M, et al. Gold nanocages as photothermal transducers for cancer treatment. *Small* 2010;**6**:811–7.
27. Dong LY, Li Y, Li Z, Xu N, Liu P, Du HY, et al. Au nanocage-strengthened dissolving microneedles for chemo-photothermal combined therapy of superficial skin tumors. *ACS Appl Mater Interfaces* 2018;**10**:9247–56.
28. Mosquera J, García I, Henriksen-Lacey M, Martínez-Calvo M, Dhanjani M, Mascareñas JL, et al. Reversible control of protein corona formation on gold nanoparticles using host-guest interactions. *ACS Nano* 2020;**14**:5382–91.
29. Kang S, Ahn S, Lee J, Kim JY, Choi M, Gujrati V, et al. Effects of gold nanoparticle-based vaccine size on lymph node delivery and cytotoxic T-lymphocyte responses. *J Control Release* 2017;**256**:56–67.
30. Liu J, Li HJ, Luo YL, Xu CF, Du XJ, Du JZ, et al. Enhanced primary tumor penetration facilitates nanoparticle draining into lymph nodes after systemic injection for tumor metastasis inhibition. *ACS Nano* 2019;**13**:8648–58.
31. Liptrott NJ, Kendall E, Nieves DJ, Farrell J, Rannard S, Fernig DG, et al. Partial mitigation of gold nanoparticle interactions with human lymphocytes by surface functionalization with a 'mixed matrix. *Nanomedicine* 2014;**9**:2467–79.
32. Xia Y, Xie YH, Yu ZS, Xiao HY, Jiang GM, Zhou XY, et al. The mevalonate pathway is a druggable target for vaccine adjuvant discovery. *Cell* 2018;**175**:1059–73.
33. Wan Y, Guo ZR, Jiang XL, Fang K, Lu X, Zhang Y, et al. Quasi-spherical silver nanoparticles: aqueous synthesis and size control by the seed-mediated Lee-Meisel method. *J Colloid Interface Sci* 2013;**394**:263–8.
34. Xia YN, Li WY, Cobley CM, Chen JY, Xia XH, Zhang Q, et al. Gold nanocages: from synthesis to theranostic applications. *Acc Chem Res* 2011;**44**:914–24.
35. You J, Zhang GD, Li C. Exceptionally high payload of doxorubicin in hollow gold nanospheres for near-infrared light-triggered drug release. *ACS Nano* 2010;**4**:1033–41.
36. Ray S, Cheng CA, Chen W, Li Z, Zink JI, Lin YY. Magnetic heating stimulated cargo release with dose control using multifunctional MR and thermosensitive liposome. *Nanotheranostics* 2019;**3**:166–78.
37. Au L, Zheng DS, Zhou F, Li ZY, Li XD, Xia YN. A quantitative study on the photothermal effect of immuno gold nanocages targeted to breast cancer cells. *ACS Nano* 2008;**2**:1645–52.
38. Skrabalak SE, Au L, Li XD, Xia YN. Facile synthesis of Ag nanocubes and Au nanocages. *Nat Protoc* 2007;**2**:2182–90.
39. Daemi S, Ashkarran AA, Bahari A, Ghasemi S. Gold nanocages decorated biocompatible amine functionalized graphene as an efficient dopamine sensor platform. *J Colloid Interface Sci* 2017;**494**:290–9.
40. Jia YP, Shi K, Yang F, Liao JF, Han RX, Yuan LP, et al. Multifunctional nanoparticle loaded injectable thermoresponsive hydrogel as NIR controlled release platform for local photothermal immunotherapy to prevent breast cancer postoperative recurrence and metastases. *Adv Funct Mater* 2020;**30**:2001059.
41. Sweeney EE, Cano-Mejia J, Fernandes R. Photothermal therapy generates a thermal window of immunogenic cell death in neuroblastoma. *Small* 2018;**14**:e1800678.
42. Wei JJ, Long Y, Guo R, Liu XL, Tang X, Rao JD, et al. Multifunctional polymeric micelle-based chemo-immunotherapy with immune checkpoint blockade for efficient treatment of orthotopic and metastatic breast cancer. *Acta Pharm Sin B* 2019;**9**:819–31.
43. Margiotta A, Frei DM, Sendstad IH, Janssen L, Neeffjes J, Bakke O. Invariant chain regulates endosomal fusion and maturation through an interaction with the SNARE Vti1b. *J Cell Sci* 2020;**133**:244624.
44. Skjeldal FM, Haugen LH, Mateus D, Frei DM, Rødseth AV, Hu X, et al. *De novo* formation of early endosomes during Rab 5-to-Rab7a transition. *J Cell Sci* 2021;**134**:254185.
45. Chen Q, Hu QY, Dukhovlinova E, Chen GJ, Ahn S, Wang C, et al. Photothermal therapy promotes tumor infiltration and antitumor activity of CAR T cells. *Adv Mater* 2019;**31**:e1900192.
46. Zhang XY, Zhang XZ, Zhang YQ, Liu MY, Jin J, Yan J, et al. Mitochondrial uncoupler triclosan induces vasorelaxation of rat arteries. *Acta Pharm Sin B* 2017;**7**:623–9.
47. Fankhauser M, Broggi MAS, Potin L, Bordry N, Jeanbart L, Lund AW, et al. Tumor lymphangiogenesis promotes T cell infiltration and potentiates immunotherapy in melanoma. *Sci Transl Med* 2017;**9**:eaal4712.
48. Sasso MS, Mitrousis N, Wang Y, Briquez PS, Hauert S, Ishihara J, et al. Lymphangiogenesis-inducing vaccines elicit potent and long-lasting T cell immunity against melanomas. *Sci Adv* 2021;**7**:eabe4362.
49. Joffre OP, Segura E, Savina A, Amigorena S. Cross-presentation by dendritic cells. *Nat Rev Immunol* 2012;**12**:557–69.
50. Yang JX, Zhang CF. Regulation of cancer-immunity cycle and tumor microenvironment by nanobiomaterials to enhance tumor immunotherapy. *Wiley Interdiscip Rev Nanomed Nanobiotechnol* 2020;**12**:e1612.
51. Shen LJ, Zhou TJ, Fan YT, Chang X, Wang Y, Sun JG, et al. Recent progress in tumor photodynamic immunotherapy. *Chin Chem Lett* 2020;**31**:1709–16.